HHS Public Access

Author manuscript

Matrix Biol. Author manuscript; available in PMC 2018 July 01.

Published in final edited form as:

Matrix Biol. 2017 July ; 60-61: 176–189. doi:10.1016/j.matbio.2016.08.011.

Nerve Guidance by a Decellularized Fibroblast Extracellular Matrix

Greg M. Harris[a], **Nicolas N. Madigan**[c], **Karen Z. Lancaster**[a], **Lynn W. Enquist**[a], **Anthony J. Windebank**[c], **Jeffrey Schwartz**[b], and **Jean E. Schwarzbauer**[a]

[a]Department of Molecular Biology, Princeton University, Princeton, NJ 08544

[b]Department of Chemistry, Princeton University, Princeton, NJ 08544

[c]Department of Neurology, Mayo Clinic, Rochester, MN 55905

Abstract

Spinal cord and peripheral nerve injuries require the regeneration of nerve fibers across the lesion site for successful recovery. Providing guidance cues and soluble factors to promote neurite outgrowth and cell survival can enhance repair. The extracellular matrix (ECM) plays a key role in tissue repair by controlling cell adhesion, motility, and growth. In this study, we explored the ability of a mesenchymal ECM to support neurite outgrowth from neurons in the superior cervical ganglia (SCG). Length and morphology of neurites extended on a decellularized fibroblast ECM were compared to those on substrates coated with laminin, a major ECM protein in neural tissue, or fibronectin, the main component of a mesenchymal ECM. Average radial neurite extension was equivalent on laminin and on the decellularized ECM, but contrasted with the shorter, curved neurites observed on the fibronectin substrate. Differences between neurites on fibronectin and on other substrates were confirmed by fast Fourier transform analyses. To control the direction of neurite outgrowth, we developed an ECM with linearly aligned fibril organization by orienting the fibroblasts that deposit the matrix on a polymeric surface micropatterned with a striped chemical interface. Neurites projected from SCGs appeared to reorient in the direction of the pattern. These results highlight the ability of a mesenchymal ECM to enhance neurite extension and to control the directional outgrowth of neurites. This micropatterned decellularized ECM architecture has potential as a regenerative microenvironment for nerve repair.

Keywords

Extracellular Matrix; Neurons; Neurite Alignment; Micropatterning

Introduction

Peripheral nerve and spinal cord injuries are a critical problem in the United States, leading to devastating functional disability, impacting long term quality of life, and causing

Correspondence to Jean E. Schwarzbauer: at: Department of Molecular Biology, Princeton University, Princeton, NJ, 08544-1014. jschwarz@princeton.edu.

Appendix A. Supplementary data: Supplementary data to this article can be found online at http://dx.doi.org/10.1016/j.matbio.2016.08.011.

significant social and economic burden for thousands of individuals each year [1]. In general, all central nervous system (CNS) injuries and most peripheral nervous system (PNS) injuries over approximately 3 cm lead to poor prognoses for recovery of neurologic function. After injury, failure to recreate the proper extracellular matrix (ECM) microenvironment to guide neurites down specific tracts can lead to insufficient axonal growth and neuronal survival resulting in scarring and poor clinical outcomes [2–4]. Inhibitory factors, wound ECM, and inflammatory cells at the lesion site do not provide the trophic support and axon guidance needed for the injured nerve cells to regenerate across a large gap [5]. Identifying a regenerative microenvironment that facilitates neurite growth by providing inductive cues and survival signals, while being devoid of inhibitory factors, could advance biomaterial design for repair of nerve injuries.

The ECM is a naturally occurring protein network that provides structure, support, and guidance to cells [6]. It also relays biological signals to the cells through specific binding sites and serves as a reservoir for soluble factors bound to ECM components. Laminins are perhaps the most significant class of ECM proteins in the nervous system, playing critical roles in both the CNS and PNS by supporting diverse functions including neuronal migration, axonal outgrowth, myelination and formation of the neuro-muscular junction [7]. In fact, laminin-111 is commonly used as the substrate of choice for neurite outgrowth assays [8–10]. However, laminins are not structural components of the ECM at injury sites. Fibronectin, on the other hand, is a major component of the wound ECM with plasma fibronectin deposited during blood coagulation and cell-derived fibronectin produced by cells in the tissue, mainly glial cells in the case of neural tissue injuries [11,12]. Surfaces coated with individual ECM proteins can promote neurite outgrowth. However, native ECM is a three-dimensional fibrillar network, and it is now well established that the architecture and mechanical properties of the ECM provide important regulatory cues to cells [13–15]. This raises the possibility that a particular combination and organization of ECM proteins may be a critical factor in determining nerve regeneration.

Fibronectin is a ubiquitous ECM protein that is a prominent component of the ECM in most tissues [11]. Fibronectin matrix is highly expressed in essentially all tissues during development, and is important for providing a scaffold to rebuild tissues after injury through its interactions with integrins and other cell receptors, as well as with collagens and many other ECM components [16]. In the nervous system, fibronectin is produced by glial cells where it promotes cell growth, survival, and motility [17]. In tissue engineering applications, fibronectin is generally used alone as a coating to make materials cell adhesive or combined with soluble factors to facilitate growth [18–20]. Studies show that a mixture of proteins may promote better neural outgrowth than single proteins [21].

We have developed a matrix decellularization procedure for mesenchymal cell-derived ECM and have shown using patterned substrates that we can develop an aligned ECM with reproducible architecture [22,23]. Linear organization of ECM has the potential to direct cell growth and orientation, which may be particularly useful for guiding neurons and their axons during regeneration. Mesenchymal cells produce a matrix that is rich in fibronectin and type I collagen but not laminin. Whether primary neurons will extend neurites across a

decellularized mesenchymal ECM to the same extent as they do on laminin substrates remains to be determined.

To show that a fibroblast-derived ECM has potential in nerve regeneration applications, we assessed neurite outgrowth on decellularized ECM compared to laminin and fibronectin substrates *in vitro*. Here we show that neurites from superior cervical ganglion (SCG) explants are able to robustly extend neurites on mesenchymal ECM. The overall morphology of SCG neurites was similar on ECM and laminin substrates, but was drastically different on fibronectin alone. Using a decellularized ECM composed of aligned matrix fibrils, both SCG explants and single cell neural cultures extended along the aligned matrix. Our results highlight the potential of spatially aligned cell-assembled ECM for use in nerve regeneration therapies.

Results

Effects of substrate on SCG neurite outgrowth

To determine the efficacy of a mesenchymal ECM in promoting neurite outgrowth, we compared neurite extension from SCGs on a surface coated with laminin-111 to extension on either a decellularized fibroblast matrix or a surface coated with fibronectin. SCG explants containing primarily sympathetic neurons and glial cells were used as the nerve cell source for their ability to extend long neurites over a laminin-coated surface in a relatively short period of time. For preparation of the decellularized ECMs, NIH 3T3 cells were cultured in the absence and presence of ascorbic acid, which promotes collagen production [24] and increases the number of type I collagen fibrils in the ECM [22]. Mesenchymal cells, such as NIH 3T3, assemble a dense ECM of diverse composition that is amenable to decellularization in contrast to neural-derived cells such as Schwann cells with which matrix assembly is very limited (Supplemental Fig. 1). SCG explants on various substrates were cultured for 1 or 3 days before fixation and staining. To visualize the full extent of neurite outgrowth and to assess neurite length, density, and morphology, overlapping images captured across each sample were assembled into a mosaic and examples for each condition are shown in Fig. 1. After one day of culture, numerous neurites had grown out of ganglia on laminin and on both decellularized ECM substrates, although neurites on laminin were obviously longer (Fig. 1). In stark contrast, neurite outgrowth from the SCG on the fibronectin substrate at one day was minimal. By three days, neurites on all substrates were evenly distributed around each explant. Projections were more similar in length on laminin and ECMs than in the one-day cultures. On the fibronectin substrate, neurite outgrowth was shorter and neurites showed a less radial direction of extension.

Quantification of neurite extension on different substrates confirmed these observations. Measurements were made of the total area covered by the SCG plus neurites and of maximum and average neurite lengths across multiple experiments. The majority of neurites extended to similar average distances on laminin and the two ECM substrates whereas projections on fibronectin were significantly shorter. The total areas, which included the area of the explant as well as the neurites, were similar on laminin and on the ECM formed without ascorbic acid (Fig. 2A). The average total area on ECM produced with ascorbic acid was about 20% smaller than on ECM without this treatment, suggesting that increasing type

I collagen in the matrix might negatively affect neurite extension for SCG neurons. The maximal distance of extension on each substrate was determined by averaging the ten longest neurites for each SCG at one and three days. The results show that neurites can extend the farthest on laminin at these time points (Fig. 2B). Laminin and decellularized ECM promoted significantly longer outgrowth than fibronectin alone, even though fibronectin is the major protein in the decellularized matrix [14]. Average neurite length was calculated by fitting an ellipse to a tracing of the outer periphery of the explant outgrowth and averaging the highest two cardinal directions per explant; this approach reduced skewing of the data by those SCGs that did not project neurites on all sides (as on day 1 Fibronectin, Fig. 1). At both 1 and 3 days, the decellularized ECM and the laminin coat supported statistically similar average neurite lengths (Fig. 2B). In contrast, neurite extension on the fibronectin substrate was statistically shorter than laminin or ECM at these times (Fig. 2B). The ECM generated with ascorbate appeared similar to laminin at 1 day but had significantly shorter average neurite length by day 3. As the ECM+ascorbate substrate did not enhance neurite outgrowth compared to ECM without ascorbate, the latter ECM was used in all subsequent experiments. The observed difference between fibronectin and the decellularized ECM in promoting neurite outgrowth suggests that neuron-fibronectin interactions may be modulated by the composition of the ECM and perhaps also its architecture.

Comparison of neurite morphologies on different substrates

Neurites on laminin or decellularized ECM projected radially out from the SCG and were organized in largely parallel arrays (Fig. 3A, B). In contrast, neurites on fibronectin were radially directed as they initially emerged from the SCG, but then appeared to develop along circuitous routes frequently crossing over other neurites (Fig. 3C). Neurites that extended beyond the neurite population continued to follow curved paths. In addition to neurite curvature, the neurites on fibronectin also varied in morphology as illustrated in high magnification images of three-day neurites stained with an α-tubulin antibody (Supplemental Fig. 2). The neurites were imaged at the periphery of the outgrowth to minimize contributions from other neural cells, which rarely migrate that far out of the SCG. Additional experiments confirmed that these are neurites, rather than support cell processes, extended from SCGs on ECM and laminin substrates by staining with antibody against phosphorylated neurofilament H, an axonal marker [25] (Supplemental Fig. 3). Neurites ranged in diameter with the largest measured at about 0.6 microns but very fine neurites are also visible. Neurites appear to merge together into bundles or branch into separate smaller neurites (Supplemental Fig. 2).

Differences in the orientations of neurites near the periphery of explants on fibronectin compared to laminin or ECM were confirmed by a fast Fourier Transform (FFT) analysis and full width-half maximum (FWHM) calculation (Fig. 4). On a laminin coat or on decellularized ECM, FFT peaks at 90° (Fig. 4B) and equivalent FWHM values (Fig. 4C) demonstrate that these substrates promote linear and generally parallel neurite directionality. In contrast, on fibronectin the FFT peak was minimal and the FWHM value was significantly higher than on the other substrates (Fig. 4B,C).

The dimensionality and architecture of the ECM distinguish it from protein-coated substrates. These features allow the ECM to provide guidance cues to neurites in three-dimensions. To investigate the organization of neurites relative to the decellularized ECM, confocal images of stained neurites and ECM were collected near the periphery of the outgrowth area (Fig. 5). Compared to the maximum intensity projection (Fig. 5A), the perspective three-dimensional view shows that neurites appear to weave over and through the fibrillar network of the decellularized ECM (Fig. 5B). To illustrate the three-dimensionality of neurite paths, the heights of neurites relative to the coverslip were determined from confocal stacksand are depth-coded in the perspective elevation view (Fig. 5C). In a sample that was 11-12 microns thick, positions of neurites covered a range of over 8 microns in the z-dimension. In a perspective view taken closer to the explant where neurite density is high and the z-dimension was over 13 microns, neurites were observed on top of and within the fibrillar ECM (Supplemental Fig. 4A). In this region, the depth-coded perspective elevation view of the neurites shows that they span a z-distance of approximately 11 microns (Supplemental Fig. 4B).

Chemical micropatterns direct ECM fibril orientation and neural cell alignment

On protein-coated surfaces, neurite outgrowth depends on cell interactions with the substrate proteins. The decellularized ECM, however, also has a three-dimensional architecture that may affect neurite extension. To determine whether neural cells are affected by the fibrillar nature of a decellularized matrix, we used an ECM with aligned matrix fibrils as a substrate. We have developed a chemical interface that can be bonded to polymer surfaces in micron-sized patterns [23]. Using photolithography, 20 × 20 micron stripes were created across the PET polymer surface (Fig. 6A). Zirconium tetra(tert-butoxide) was vapor-deposited onto the surface and then warmed to create a ZrO_2 layer before incubation in 1 mM 1,4-butanediphosphonic acid to yield a self-assembled monolayer of phosphonates (SAMP), which provides a cell adhesive surface (Fig. 6B). This chemical layer is very thin, less than 70 nm.

NIH 3T3 cells attach along the ZrO_2/SAMP stripes, grow to confluence in alignment, and assemble a dense ECM with fibrils oriented in the direction of the striped pattern (Supplemental Fig. 5). To determine the effect of ECM fibrils on the orientations of individual neural cells, C6-R radial glial cells were allowed to attach and spread on a decellularized matrix (Fig. 6C). When the matrix fibrils were aligned with a pattern, the glial cells spread in the direction of the fibrils and the chemical pattern. Cells spread in all directions on the unpatterned decellularized matrix. When radial glial cells were plated and differentiated PC12 cells were added after 2 days and cultured for 3 days together on the aligned ECM, rhodamine-phalloidin staining shows a high degree of alignment of cells and PC12-derived neurites with patterned ECM fibrils (Fig. 6C). On unpatterned ECM, cells and neurites showed no spatial directionality. These results demonstrate the ability of a patterned ECM to control the orientations of cells and neurites across a polymeric material.

SCG neurite outgrowth on patterned decellularized ECM

The effect of ECM fibril alignment on neurite extension was evaluated using SCG explants. Explants cultured for 3 days showed nearly symmetrical radial outgrowth of neurites from

the SCG (Figs. 1, 7A). On aligned ECM, however, neurites that initially projected perpendicular to the striped pattern appeared to turn in the direction of the pattern as they grew radially from the SCG (Fig. 7B). The overall shape of explants with neurites was gauged by calculating the average aspect ratio from multiple samples. On patterned ECM, the average aspect ratio was 1.40, statistically different from the aspect ratio on unpatterned ECM at 1.06, which is essentially circular (Fig. 7C). The higher aspect ratio indicates shorter neurites in the direction perpendicular to the pattern. Average neurite length was measured parallel and perpendicular to the direction of the pattern. Neurites extended parallel to the pattern were the same length as their unpatterned counterparts, while neurites did not extend as far when perpendicular to the pattern (Fig. 7D). Higher magnification images at the periphery indicate curvature of the neurites on the axis of the ellipse perpendicular to the pattern but not on the axis parallel to the pattern (Supplemental Fig. 6). These results indicate that the neurites exhibit a directional response to the patterned ECM fibrils.

Discussion

Nerve regeneration across injury sites requires appropriate guidance and survival cues provided by ECM proteins and neurotrophic factors. The composition and architecture of the fibronectin-rich matrices that form after injury and during tissue repair differ from the ECM found in undamaged neural tissue [26]. Therefore, we set out to assess the ability of a mesenchymal ECM to promote neurite outgrowth. Our results show that, on average, SCG primary neurons extended neurites similar distances on laminin and decellularized ECM substrates, but that neurites were shorter and less linear on a fibronectin substrate. Using decellularized ECM with fibrils aligned with a striped micropattern, we found that radial glial cells and neurites from differentiated PC12 cells followed the orientation of the ECM. Patterned ECM also affected the projection of neurites from SCG explants. These results show that the orientation of ECM fibrils guides the direction of neurite outgrowth, which should have applications in the repair and regeneration of nervous tissue.

ECM proteins alone and in combination have been compared for their effects on neural cell adhesion and neurite outgrowth *in vitro*. Results have differed depending on the specific proteins, how they were presented, and what types of neurons or glia were tested. For example, astrocyte migration was promoted on a laminin substrate but arrested on fibronectin [27]. Sensory neurons preferred a collagen matrix containing laminin over fibronectin for neurite outgrowth, whereas motor neurons preferred collagen enriched with fibronectin [28]. Neurite outgrowth from adult brain neurons was greater on fibronectin than on laminin [29]. We found neurites extended from embryonic SCG neurons were significantly longer on laminin-coated than on fibronectin-coated substrates. While the average outgrowth length was similar on laminin and decellularized ECM, the maximum neurite length was higher on laminin. NIH 3T3 cell-derived ECM contains some laminin-111 prior to decellularization, but laminin appears diminished after decellularization (unpublished observations). Fibronectin is by far the most abundant protein in the decellularized matrix [14]. Therefore, it seems likely that the composition and/or the architecture of the ECM can modulate the effects of fibronectin on neurite outgrowth. The architecture of the ECM provides a fibrillar pathway for growth cone motility that could

facilitate neurite elongation and the rate of elongation might depend on the composition of the fibrils. Fibroblasts express tenascin-C [30], which is known to reduce cell adhesion by binding to fibronectin [31] and which has been implicated in enhancing neurite outgrowth in vivo [32]. Neural cells express integrin receptors for laminins [33,34] and fibronectin [35–38] making coordinated engagement of different integrins another mechanism to control neurite outgrowth on an ECM substrate. In peripheral nerve injuries, fibroblasts and Schwann cells are responsible for producing a new ECM to guide cell migration and axon regeneration over the injury gap [39]. Perhaps by optimizing the architecture and composition of the ECM, one could create a permissive environment to control neurite adhesion and outgrowth guidance.

In addition to neurite outgrowth, we also observed a difference in neurite morphology on fibronectin compared to laminin. Rather than projecting linearly from the SCG, neurites on fibronectin-coated surfaces showed a more randomized outgrowth path. Several factors could explain the morphological differences in neurites on fibronectin. Higher levels of fibronectin receptors compared to laminin receptors would reduce the speed of outgrowth [40]. Schwann cells or other support cells in the SCG may show enhanced motility on fibronectin leading to more out-migration from the explant; closer contact of glial cells with the neurites has previously been shown to affect axon diameters [41,42]. Neurites also appeared to interact with each other and intertwine which could have an impact on the direction or persistence of outgrowth.

Our technology for controlling neurite alignment utilizes a robust, micropatterned surface chemistry to orient cells and their cell-assembled natural ECM fibrils [22]. Other methods of neurite guidance have been described, including synthetic materials engineered to have ridges, pillars, or posts to provide topological cues [43–46], or mechanical cues arising from patterning surfaces of defined rigidity and guidance such as porous or electrospun materials [47,48]. In contrast to these other engineering methods, using a cell-assembled ECM provides a potentially more complete regenerative microenvironment with multiple ECM proteins, three-dimensional architecture, and binding sites for neurotrophic growth factors. Our results show the ability of oriented ECM fibrils to control the direction of neuronal projections and also demonstrate the efficacy of the aligned ECM to promote oriented adhesion of multiple nerve cell types. Thus an aligned decellularized ECM could be used to develop biomaterials that target neurites to specific destinations for nerve repair strategies.

Experimental Procedures

Dissection of Superior Cervical Ganglia

SCGs containing primary embryonic sympathetic neurons were obtained from Sprague-Dawley rats (embryonic day 15.5 - 16.5, Hilltop Labs Incorporated, Pennsylvania, United States). A detailed procedure can be found elsewhere [49,50], but briefly, for each study, the animal was euthanized and handled in strict accordance with good animal practice as defined by the relevant national and local animal welfare bodies, and approved by the Princeton University Institutional Animal Care and Use Committee (IACUC). Superior cervical ganglia (SCG) were harvested from the base of the neck opposite the second and third cervical vertebrae and maintained in whole form. Ganglia were cultured in growth

medium, which consisted of neurobasal medium (Life Technologies) containing 1% B-27 medium supplement (Life Technologies), 1% Pen Strep Glutamine (Life Technologies), and 50 ng/mL Nerve Growth Factor 2.5S (NGF) (Invitrogen). The medium was filtered using a 0.22 μm filter prior to addition of NGF (Stericup filter unit, Millipore). Ganglia could be stored up to one week in Hibernate-E reagent (Life Technologies).

Cell Culture and Substrate Preparation

NIH 3T3 cells (ATCC, Manassas, VA) and GFP-expressing C6-R radial glial cell line derived from C6 glioma cells (kindly provided by Dr. Martin Grumet, Rutgers University) [51] were cultured in DMEM (Hyclone, Logan UT) supplemented with 10% bovine calf serum (Hyclone, Logan, UT) and 1% penicillin/streptomycin. PC12 cells were cultured in RPMI 1640 Basal medium supplemented with 10% horse serum, 5% fetal bovine serum, and 1 % penicillin/streptomycin and differentiated using RPMI 1640 basal media supplemented with 1% horse serum and 100 ng/ml NGF. For differentiation, PC12 cells were grown to approximately 60% confluence and differentiation medium was added. Medium was changed every 3 days for 12 days to allow differentiation of cells and extension of neurites.

For protein coating of coverslips, fibronectin was purified from fresh, frozen rat plasma by gelatin-Sepharose affinity chromatography. Fibronectin in PBS and laminin (Life Technologies) in Hanks Balanced salt solution (HBSS) were incubated on coverslips at 10 μg/ml overnight at 37 °C and washed twice with PBS before seeding SCG explants. Ganglia were cultured on surfaces up to 3 days before fixation.

Using decellularized matrix as a substrate, radial glial cells were seeded at 25,000 cells/cm^2, cultured for 2 days and then fixed. For co-culture with PC12 cells, radial glial cells were cultured for 2 days on decellularized ECM. Differentiated PC12 cells were then seeded in the decellularized matrix/radial glial cell culture at 8,000 cells/cm^2 in differentiation medium and cultured for 3 days before fixing and staining.

Micropatterning on Polyethylene Teraphlalate (PET)

PET was micropatterned using photolithography and a chemical vapor deposition-based sequence to create 20×20 micron stripes as described previously [23]. In short, hexamethyldisilazane (Sigma Aldrich, Milwaukee, WI) was spin-cast onto a 0.05 mm thick PET polymer (Goodfellow Corporation, Oakdale, PA) surface followed by spin-casting AZ-5214E photoresist (Clariant Corporation, Holden, MA). After exposure to UV light (365 nm, 4 W) through a photomask, the surface was developed in AZ-312 MIF (Clariant Corporation, Holden, MA). The substrates were washed in deionized water and then placed inside a glass deposition chamber. After evacuation of the chamber, samples were exposed to vapor of zirconium tetra(*tert*-butoxide), warmed to form the crosslinked zirconium oxide base layer, and then back-filled with zero-grade nitrogen prior to dismounting. Substrates were then soaked in an ethanol solution of 1,4-butanediphosphonic acid (0.25 mg/mL) for 24 hours to bond a monolayer of phosphonate in patterned stripes across the entire substrate. The substrates were rinsed sequentially with ethanol and 2-propanol, dried under nitrogen, and inspected by optical microscopy.

Preparation of Decellularized ECM

All glass and PET surfaces were treated with 70% ethanol for 20 minutes and then washed three times with PBS before use. To create unpatterned decellularized ECM, NIH 3T3 cells were seeded on glass coverslips at 75,000 cells/cm^2 and grown for 6 days, changing medium every other day before decellularization. Ascorbic acid (50 μg/ml) was added on days 3 and 5 for selected groups. On PET patterns, cells were plated at 25,000 cells/cm^2 in DMEM. After four hours, unattached cells were removed and DMEM with 10% bovine calf serum was added. Cells were cultured for 10 days to allow cells to grow to confluency and assemble a dense fibronectin matrix before decellularization, which was performed as previously described [14]. After the final wash, matrices were observed by phase microscopy to confirm successful cell removal and the presence of intact ECM on the coverslip and stored in PBS for at least 1 week at 4 °C.

Immunofluorescence and Microscopy

All samples were fixed with 3.7% formaldehyde in PBS and neuronal samples were permeabilized using 1% Triton-X100 in PBS. Cell-assembled ECM was incubated with R457 rabbit anti-fibronectin polyclonal antiserum (1:100) followed by either fluorescein-conjugated or rhodamine-conjugated goat anti-rabbit IgG (1:600) to observe fibronectin fibrils. R457 antiserum was raised against the N-terminal 70 kDa fragment of rat fibronectin [52]. SCG neurites were visualized using monoclonal anti-α-tubulin (1:500) (Clone-B-5-1-2, Sigma) followed by fluorescein-conjugated goat anti-mouse IgG (1:600). SCG axons were visualized using a mouse monoclonal antibody against phosphorylated neurofilament H (SMI 31, Abcam) (1:400) followed by fluorescein-conjugated goat anti-mouse IgG (1:600). PC12 neurites were visualized using rhodaminephalloidin (1:100) to observe F-actin. All antibody incubations were done for 30 minutes at 37 °C. Coverslips were mounted using ProLong Gold anti-fade reagent (Life Technologies, Grand Island, NY).

Samples were analyzed with a Nikon Eclipse Ti inverted microscope equipped with a Hamamatsu C10600 ORCA-R2 digital camera and iVision software. For SCG explants, iVision software with a dedicated script was utilized to take images with a 10× objective tiled over a large area to create a mosaic view of explant and outgrowth. For neurite width measurements, images were taken using a Nikon structured illumination based super-resolution microscope (N-SIM) with 100× objective on ganglia cultured 3 days. Images were reconstructed and analyzed using Nikon Elements and ImageJ software.

To measure maximal neurite lengths, the 10 longest neurites from each explant were measured from the explant edge to the end of the neurite in a straight line. These measurements were averaged for each sample in each condition. Neurite lengths from a total of 3-6 explants from at least 3 independent experiments were averaged. Average neurite lengths were measured by tracing the outer boundary of neurites in ImageJ and fitting the tracing to an ellipse. Measurements were then made from the SCG to the edge in each quadrant of the ellipse and the 2 longest measurements were averaged for each explant. For the total area of SCG plus neurites, the perimeter of the SCG with neurites was traced and fit to an ellipse, and the area within the perimeter was measured using ImageJ. The shape of SCG plus neurites on patterned and unpatterned ECM was quantified by fitting the total

neurite plus SCG area with an ellipse and calculating the aspect ratio of the resulting ellipse. Neurite widths were measured from 2 different explants per condition and 3 images per explant. The two apparently largest neurites in field were measured along the neurite for the width and averaged for each condition.

Alignment of fibronectin fibrils was quantified by fast Fourier transform (FFT) analysis of cropped images (1024 × 1024 pixels) using ImageJ [22,53]. FFT data were used to calculate the full width-half maximum (FWHM) value for each curve, which was used for comparison across samples. FFT analysis quantifies the degree of alignment of the fluorescent signal (i.e., fibronectin fibrils) with a peak at 90 degrees signifying alignment with the underlying pattern. The FWHM calculation is the width of the FFT curve at half of the maximum peak value and provides a way to directly compare samples.

Statistics

ANOVA analysis was run to determine statistical significance of differences between sample groups and Student t tests were run to determine significance between two individual samples. The data was considered statistically significant when $p < 0.05$.

Supplementary Material

Refer to Web version on PubMed Central for supplementary material.

Acknowledgments

The authors gratefully acknowledge support from the National Institutes of Health (R01CA160611 to JES, R01NS33506 and R01NS060699 to LWE), the New Jersey Commission on Spinal Cord Research (CSCR15IRG002 to JES), and a New Ideas in the Natural Sciences award from the Princeton Dean for Research (to JES and JS). GMH and NNM were supported by NIH T32 Post-doctoral Training Grant T32EB005583 (to the New Jersey Center for Biomaterials). We thank Dr. Martin Grumet (Rutgers University) for kindly supplying GFP-tagged C6-R radial glial cells and Dr. Peter Yurchenco (Rutgers--Robert Wood Johnson Medical School) for anti-laminin-111 antibodies. The authors are grateful to Dr. Gary Laevsky, director of the Molecular Biology Confocal Microscopy Core Facility, a Nikon Center of Excellence, for scientific and technical assistance.

References

1. Bekelis K, Missios S, Spinner RJ. Falls and peripheral nerve injuries: an age-dependent relationship. J Neurosurg. 2015; 123:1223–1229. [PubMed: 25978715]
2. Noble J, Munro CA, Prasad VS, Midha R. Analysis of upper and lower extremity peripheral nerve injuries in a population of patients with multiple injuries. J Trauma. 1998; 45:116–122. [PubMed: 9680023]
3. Brown RA, Phillips JB. Cell responses to biomimetic protein scaffolds used in tissue repair and engineering. Int Rev Cytol. 2007; 262:75–150. [PubMed: 17631187]
4. Nectow AR, Marra KG, Kaplan DL. Biomaterials for the development of peripheral nerve guidance conduits. Tissue Eng Part B Rev. 2012; 18:40–50. [PubMed: 21812591]
5. Deumens R, Bozkurt A, Meek MF, Marcus MA, Joosten EA, Weis J, Brook GA. Repairing injured peripheral nerves: Bridging the gap. Prog Neurobiol. 2010; 92:245–276. [PubMed: 20950667]
6. Frantz C, Stewart KM, Weaver VM. The extracellular matrix at a glance. J Cell Sci. 2010; 123:4195–4200. [PubMed: 21123617]
7. Barros CS, Franco SJ, Muller U. Extracellular Matrix: Functions in the Nervous System. Cold Spring Harb Perspect Biol. 2011; 3

8. Hsu SH, Kuo WC, Chen YT, Yen CT, Chen YF, Chen KS, Huang WC, Cheng H. New nerve regeneration strategy combining laminin-coated chitosan conduits and stem cell therapy. Acta Biomater. 2013; 9:6606–6615. [PubMed: 23376237]
9. Junka R, Valmikinathan CM, Kalyon DM, Yu XJ. Laminin Functionalized Biomimetic Nanofibers for Nerve Tissue Engineering. J Biomater Tissue Eng. 2013; 3:494–502. [PubMed: 24083073]
10. Neal RA, Tholpady SS, Foley PL, Swami N, Ogle RC, Botchwey EA. Alignment and composition of laminin-polycaprolactone nanofiber blends enhance peripheral nerve regeneration. J Biomed Mater Res A. 2012; 100a:406–423.
11. Mao Y, Schwarzbauer JE. Fibronectin fibrillogenesis, a cell-mediated matrix assembly process. Matrix Biol. 2005; 24:389–399. [PubMed: 16061370]
12. Volpato FZ, Fuhrmann T, Migliaresi C, Hutmacher DW, Dalton PD. Using extracellular matrix for regenerative medicine in the spinal cord. Biomaterials. 2013; 34:4945–4955. [PubMed: 23597407]
13. Engler AJ, Chan M, Boettiger D, Schwarzbauer JE. A novel mode of cell detachment from fibrillar fibronectin matrix under shear. J Cell Sci. 2009; 122:1647–1653. [PubMed: 19401337]
14. Mao Y, Schwarzbauer JE. Stimulatory effects of a three-dimensional microenvironment on cell-mediated fibronectin fibrillogenesis. J Cell Sci. 2005; 118:4427–4436. [PubMed: 16159961]
15. Cukierman E, Pankov R, Stevens DR, Yamada KM. Taking cell-matrix adhesions to the third dimension. Science. 2001; 294:1708–1712. [PubMed: 11721053]
16. Singh P, Carraher C, Schwarzbauer JE. Assembly of Fibronectin Extracellular Matrix. Annu Rev Cell Dev Biol. 2010; 26:397–419. [PubMed: 20690820]
17. Baronvanevercooren A, Kleinman HK, Seppa HEJ, Rentier B, Duboisdalcq M. Fibronectin Promotes Rat Schwann-Cell Growth and Motility. J Cell Biol. 1982; 93:211–216. [PubMed: 7040414]
18. Mosahebi A, Wiberg M, Terenghi G. Addition of fibronectin to alginate matrix improves peripheral nerve regeneration in tissue-engineered conduits. Tissue Eng. 2003; 9:209–218. [PubMed: 12740084]
19. Han H, Ao Q, Chen G, Wang S, Zuo H. A novel basic fibroblast growth factor delivery system fabricated with heparin-incorporated fibrin-fibronectin matrices for repairing rat sciatic nerve disruptions. Biotechnol Lett. 2010; 32:585–591. [PubMed: 20033834]
20. King VR, Henseler M, Brown RA, Priestley JV. Mats made from fibronectin support oriented growth of axons in the damaged spinal cord of the adult rat. Exp Neurol. 2003; 182:383–398. [PubMed: 12895449]
21. Chen YS, Hsieh CL, Tsai CC, Chen TH, Cheng WC, Hu CL, Yao CH. Peripheral nerve regeneration using silicone rubber chambers filled with collagen, laminin and fibronectin. Biomaterials. 2000; 21:1541–1547. [PubMed: 10885726]
22. Singh S, Bandini SB, Donnelly PE, Schwartz J, Schwarzbauer JE. A cell-assembled, spatially aligned extracellular matrix to promote directed tissue development. J Mater Chem B. 2014; 2:1449–1453.
23. Donnelly PE, Jones CM, Bandini SB, Singh S, Schwartz J, Schwarzbauer JE. A Simple Nanoscale Interface Directs Alignment of a Confluent Cell Layer on Oxide and Polymer Surfaces. J Mater Chem B. 2013; 1:3553–3561.
24. Boyera N, Galey I, Bernard BA. Effect of vitamin C and its derivatives on collagen synthesis and cross-linking by normal human fibroblasts. Int J Cosmet Sci. 1998; 20:151–158. [PubMed: 18505499]
25. Tomishima MJ, Enquist LW. A conserved alpha-herpesvirus protein necessary for axonal localization of viral membrane proteins. J Cell Biol. 2001; 154:741–752. [PubMed: 11502759]
26. Silver J, Miller JH. Regeneration beyond the glial scar. Nat Rev Neurosci. 2004; 5:146–156. [PubMed: 14735117]
27. Johnson KM, Milner R, Crocker SJ. Extracellular matrix composition determines astrocyte responses to mechanical and inflammatory stimuli. Neurosci Lett. 2015; 600:104–109. [PubMed: 26067407]
28. Gonzalez-Perez F, Ale A, Santos D, Barwig C, Freier T, Navarro X, Udina E. Substratum preferences of motor and sensory neurons in postnatal and adult rats. Eur J Neurosci. 2016; 43:431–442. [PubMed: 26332537]

29. Tonge DA, de Burgh HT, Docherty R, Humphries MJ, Craig SE, Pizzey J. Fibronectin supports neurite outgrowth and axonal regeneration of adult brain neurons in vitro. Brain Res. 2012; 1453:8–16. [PubMed: 22483961]
30. Desai VD, Hsia HC, Schwarzbauer JE. Reversible Modulation of Myofibroblast Differentiation in Adipose-Derived Mesenchymal Stem Cells. PLoS One. 2014:9.
31. Midwood KS, Valenick LV, Hsia HC, Schwarzbauer JE. Coregulation of fibronectin signaling and matrix contraction by tenascin-C and syndecan-4. Mol Biol Cell. 2004; 15:5670–5677. [PubMed: 15483051]
32. Schweitzer J, Becker T, Lefebvre J, Granato M, Schachner M, Becker CG. Tenascin-C is involved in motor axon outgrowth in the trunk of developing zebrafish. Dev Dyn. 2005; 234:550–566. [PubMed: 16110513]
33. Plantman S, Patarroyo M, Fried K, Domogatskaya A, Tryggvason K, Hammarberg H, Cullheim S. Integrin-laminin interactions controlling neurite outgrowth from adult DRG neurons in vitro. Mol Cell Neurosci. 2008; 39:50–62. [PubMed: 18590826]
34. Tomaselli KJ, Doherty P, Emmett CJ, Damsky CH, Walsh FS, Reichardt LF. Expression of beta 1 integrins in sensory neurons of the dorsal root ganglion and their functions in neurite outgrowth on two laminin isoforms. J Neurosci. 1993; 13:4880–4888. [PubMed: 7693896]
35. Haack H, Hynes RO. Integrin receptors are required for cell survival and proliferation during development of the peripheral glial lineage. Dev Biol. 2001; 233:38–55. [PubMed: 11319856]
36. Milner R, Wilby M, Nishimura S, Boylen K, Edwards G, Fawcett J, Streuli C, Pytela R, ffrenchConstant C. Division of labor of Schwann cell integrins during migration on peripheral nerve extracellular matrix ligands. Dev Biol. 1997; 185:215–228. [PubMed: 9187084]
37. Wakatsuki S, Araki T, Sehara-Fujisawa A. Neuregulin-1/glial growth factor stimulates Schwann cell migration by inducing alpha 5 beta 1 integrin-ErbB2-focal adhesion kinase complex formation. Genes Cells. 2014; 19:66–77. [PubMed: 24256316]
38. Vogelezang MG, Liu Z, Relvas JB, Raivich G, Scherer SS, ffrench-Constant C. Alpha4 integrin is expressed during peripheral nerve regeneration and enhances neurite outgrowth. J Neurosci. 2001; 21:6732–6744. [PubMed: 11517262]
39. Richard L, Vedrenne N, Vallat JM, Funalot B. Characterization of Endoneurial Fibroblast-like Cells from Human and Rat Peripheral Nerves. J Histochem Cytochem. 2014; 62:424–435. [PubMed: 24670794]
40. Palecek SP, Loftus JC, Ginsberg MH, Lauffenburger DA, Horwitz AF. Integrin-ligand binding properties govern cell migration speed through cell-substratum adhesiveness. Nature. 1997; 385:537–540. [PubMed: 9020360]
41. Windebank AJ, Wood P, Bunge RP, Dyck PJ. Myelination Determines the Caliber of Dorsal-Root Ganglion Neurons in Culture. J Neurosci. 1985; 5:1563–1569. [PubMed: 4009246]
42. Pannese E, Ledda M, Matsuda S. Nerve-Fibers with Myelinated and Unmyelinated Portions in Dorsal Spinal Roots. J Neurocytol. 1988; 17:693–700. [PubMed: 3210047]
43. Xie JW, MacEwan MR, Liu WY, Jesuraj N, Li XR, Hunter D, Xia YN. Nerve Guidance Conduits Based on Double-Layered Scaffolds of Electrospun Nanofibers for Repairing the Peripheral Nervous System. ACS Appl Mater Interfaces. 2014; 6:9472–9480. [PubMed: 24806389]
44. Cai L, Zhang L, Dong JY, Wang SF. Photocured Biodegradable Polymer Substrates of Varying Stiffness and Microgroove Dimensions for Promoting Nerve Cell Guidance and Differentiation. Langmuir. 2012; 28:12557–12568. [PubMed: 22857011]
45. Hoffman-Kim D, Mitchel JA, Bellamkonda RV. Topography, Cell Response, and Nerve Regeneration. Annu Rev Biomed Eng. 2010; 12:203–231. [PubMed: 20438370]
46. Johansson F, Carlberg P, Danielsen N, Montelius L, Kanje M. Axonal outgrowth on nano-imprinted patterns. Biomaterials. 2006; 27:1251–1258. [PubMed: 16143385]
47. Phillips JB, Brown R. Micro-structured Materials and Mechanical Cues in 3D Collagen Gels. Methods Mol Biol. 2011; 695:183–196. [PubMed: 21042973]
48. Grinnell F. Fibroblast biology in three-dimensional collagen matrices. Trends Cell Biol. 2003; 13:264–269. [PubMed: 12742170]
49. Zareen N, Greene LA. Protocol for culturing sympathetic neurons from rat superior cervical ganglia (SCG). J Vis Exp. 2009

50. Curanovic D, Ch'ng TH, Szpara M, Enquist L. Compartmented neuron cultures for directional infection by alpha herpesviruses. Curr Protoc Cell Biol. 2009 Chapter 26Unit 26 24.

51. Hormigo A, McCarthy M, Nothias JM, Hasegawa K, Huang W, Friedlander DR, Fischer I, Fishell G, Grumet M. Radial glial cell line C6-R integrates preferentially in adult white matter and facilitates migration of coimplanted neurons in vivo. Exp Neurol. 2001; 168:310–322. [PubMed: 11259119]

52. Aguirre KM, McCormick RJ, Schwarzbauer JE. Fibronectin self-association is mediated by complementary sites within the amino-terminal one-third of the molecule. J Biol Chem. 1994; 269:27863–27868. [PubMed: 7961716]

53. Huang CY, Fu XL, Liu J, Qi YM, Li SH, Wang HJ. The involvement of integrin beta 1 signaling in the migration and myofibroblastic differentiation of skin fibroblasts on anisotropic collagen-containing nanofibers. Biomaterials. 2012; 33:1791–1800. [PubMed: 22136719]

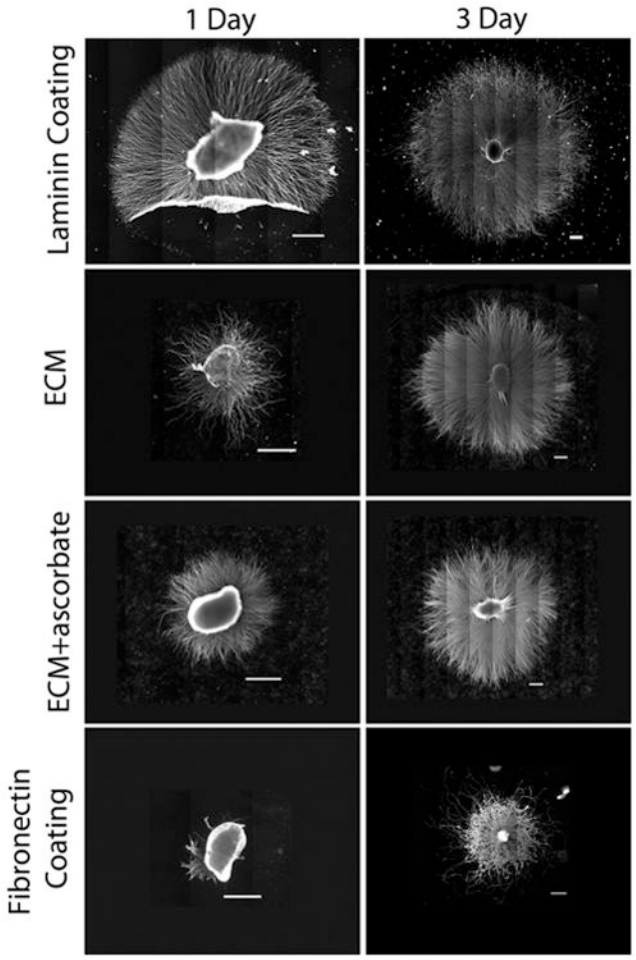

Fig. 1.

Neurite extension from SCG explants. SCGs were placed on the indicated substrates and cultured for 1 or 3 days to allow neurite outgrowth. Explants were stained with anti-α-tubulin antibody. Multiple images were captured across each sample and were subsequently assembled into a mosaic to show total neurite outgrowth. SCGs and neurites tend to be more loosely attached to laminin than to the other substrates resulting in frequent folding over of neurites during the staining procedure (as in the laminin 1 day sample). Scale bars are 500 microns.

A

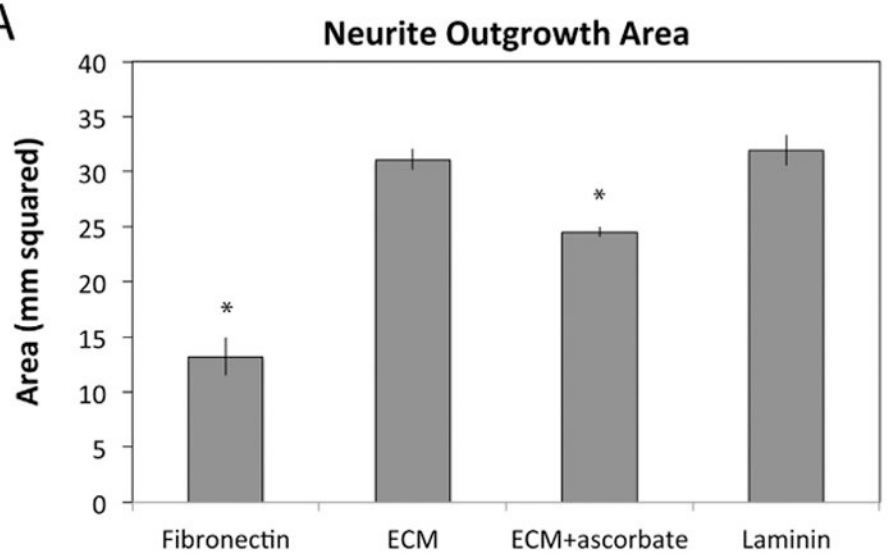

B

	1 Day Outgrowth (microns)		3 Day Outgrowth (microns)	
Protein Coating	Average Length	Maximum Length	Average Length	Maximum Length
Fibronectin	342.8 ± 46.4*	481.4 ± 48.8*	1637.4 ± 91.7*	2343.4 ± 126.4*
ECM	549.0 ± 58.1	704.6 ± 49.0*	2588.1 ± 79.0	2995.0 ± 74.3*
ECM+ascorbate	757.9 ± 131.0	800.3 ± 50.1*	2207.8 ± 37.0*	2712.8 ± 42.7*
Laminin	831.9 ± 116.0	1006.3 ± 44.4	2937.7 ± 106.2	3955.8 ± 198.9

Fig. 2.

Quantitative analysis of neurite outgrowth. (A) The total outgrowth area of SCG plus neurites was measured for between 3 and 6 explants per substrate. Bars show average areas ± standard error. (B) The length of the majority of neurites (average length) and the average length of the 10 longest neurites (maximum length) were measured on days 1 and 3 for each of between 3 and 6 explants per substrate. The table shows these measurements for each condition ± standard error. Samples from at least 3 independent experiments are shown. Significance relative to laminin was calculated with * indicating $p < 0.05$.

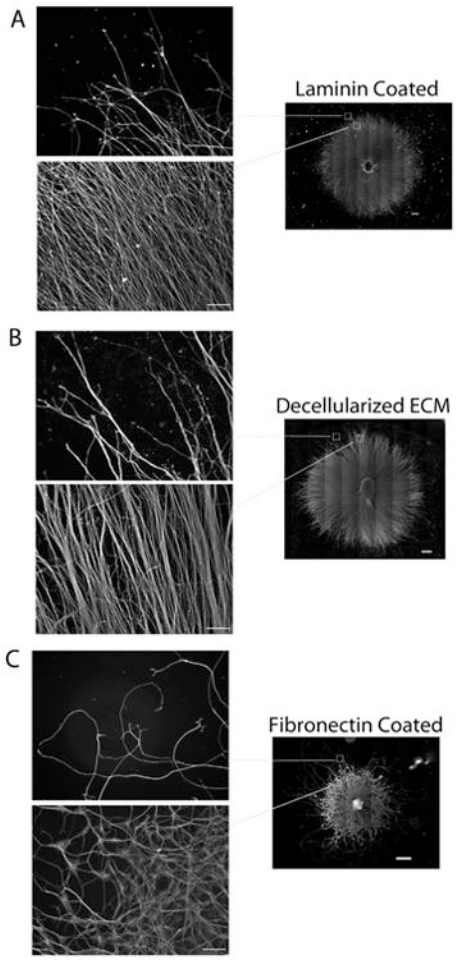

Fig. 3.

Comparison of neurite outgrowth patterns. Areas near the edge and beyond the edge of the majority of neurites in mosaic images (from Fig. 1) were selected (boxed regions in righthand images) and magnified for each substrate. Neurites on laminin (A) and decellularized ECM (B) show similar radial outgrowth paths in contrast to neurites on fibronectin (C), which were less persistent in the direction of extension. Scale bars are 500 microns on mosaics and 100 microns on higher magnification images of neurites.

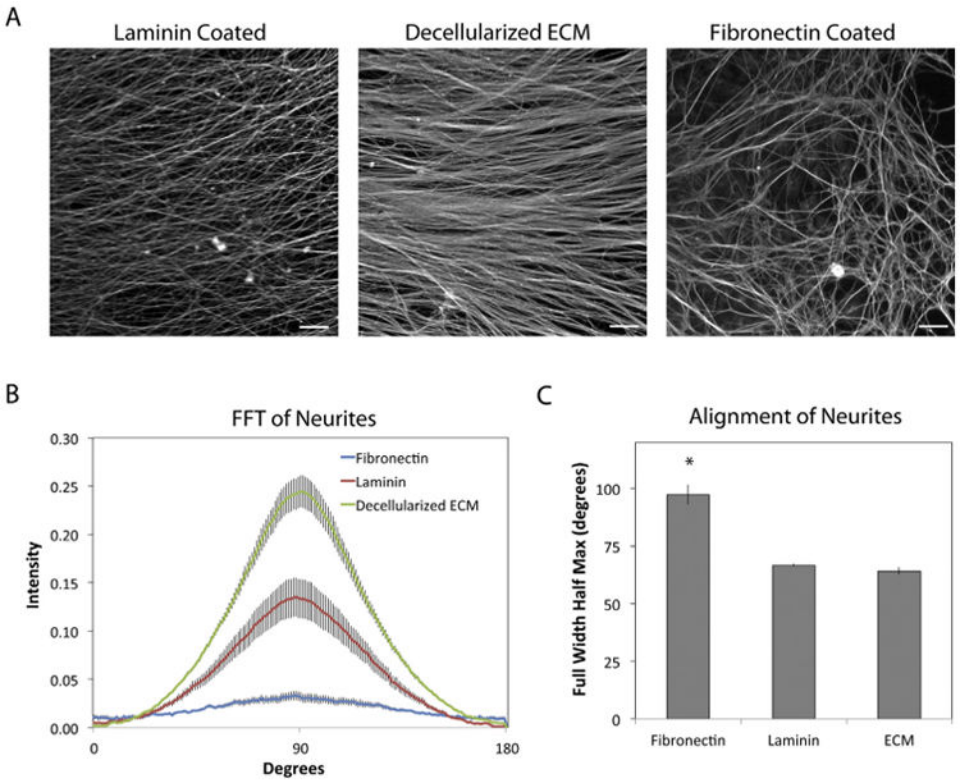

Fig. 4.

FFT analysis of neurite orientations. (A) SCGs and neurites were stained with anti-α-tubulin antibodies at 3 days of culture on the indicated substrates. Regions near the edges of the majority of neurites were selected at random from immunofluorescence images. Representative regions are shown. (B) The orientation of neurites was quantified by a FFT analysis of fluorescence images. Radial intensity data were plotted from 0° to 180° and show the range of values for 5 images in one explant per condition. (C) The full width-half maximum (FWHM) value of each pixel intensity curve was calculated. Scale bars are 100 microns. Error bars show the average of the 5 curves ± standard error. * indicates $p < 0.05$.

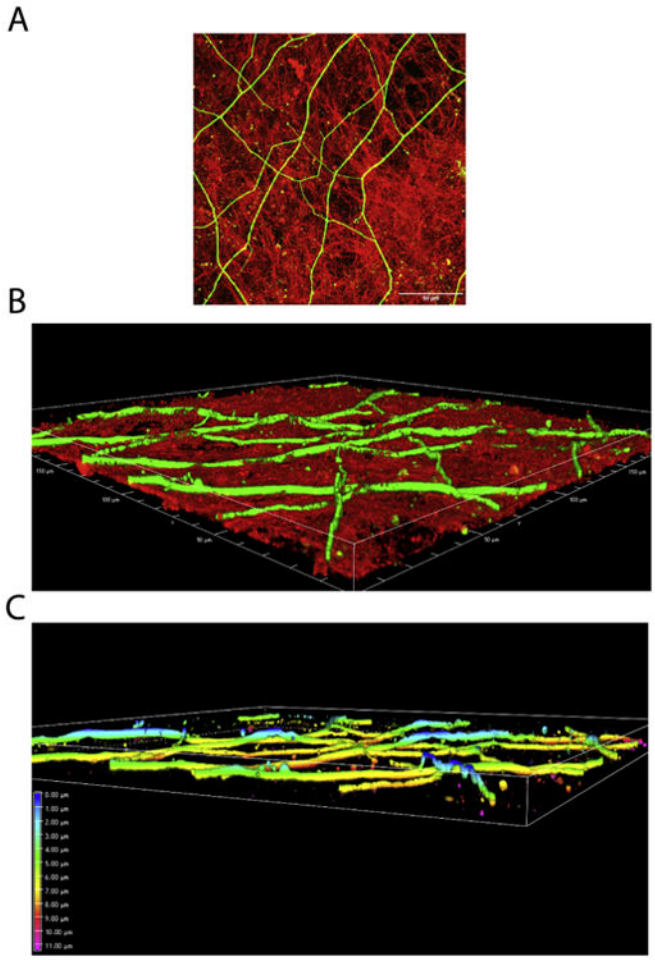

Fig. 5.

Effects of ECM dimensionality and architecture on neurites. (A) Neurites extended on decellularized ECM were stained with an anti-α-tubulin monoclonal antibody followed by fluorescein-goat anti-mouse IgG. The ECM was stained with R457 anti-fibronectin antiserum and rhodamine-goat anti-rabbit IgG. A merged image of confocal z-sections from the periphery of the explant is shown. Scale bar is 50 microns. (B) A perspective 3D view of the confocal z-stack for the image in A is shown. Sample is ~ 12 microns thick. (C) The perspective 3D view from B was depth-coded for the neurites only. Colors represent different levels of depth within the sample with those regions of neurites that are the highest in blue (0 microns) and the yellow regions indicating neurites that are within the ECM (7-8 microns from the top).

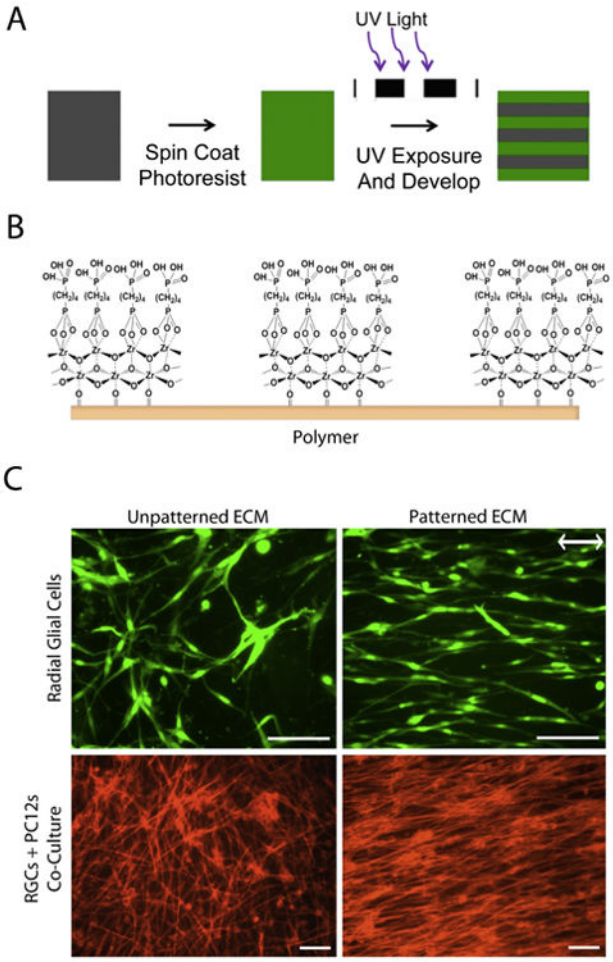

Fig. 6.

Patterning of ECM and neural cells. (A) The schematic shows the steps in soft lithography of photoresist onto PET polymers to create stripes. Photoresist is spin-coated onto polymer, cured with UV light through a photomask, and developed leaving 20 × 20 micron stripes across the entire polymer surface. (B) Surface chemistry modification of the PET polymer with photoresist involves deposition of zirconium tetra(tert butoxide) followed by incubation in phosphonic acid which bonds to the ZrO_2 to form a cell-friendly self-assembled layer of phosphonates (SAMP) in striped patterns. (C, top) GFP-tagged radial glial cells were seeded onto unpatterned or patterned ECM, grown for 2 days, and then images of GFP were captured. Double headed arrow indicates the direction of the striped pattern. (C, bottom) GFP-tagged radial glial cells (RGCs) were grown for 2 days on unpatterned or patterned decellularized ECM, then differentiated PC12 cells were added and after an additional 3 days, cultures were stained with rhodamine-phalloidin. Scale bars are 100 microns.

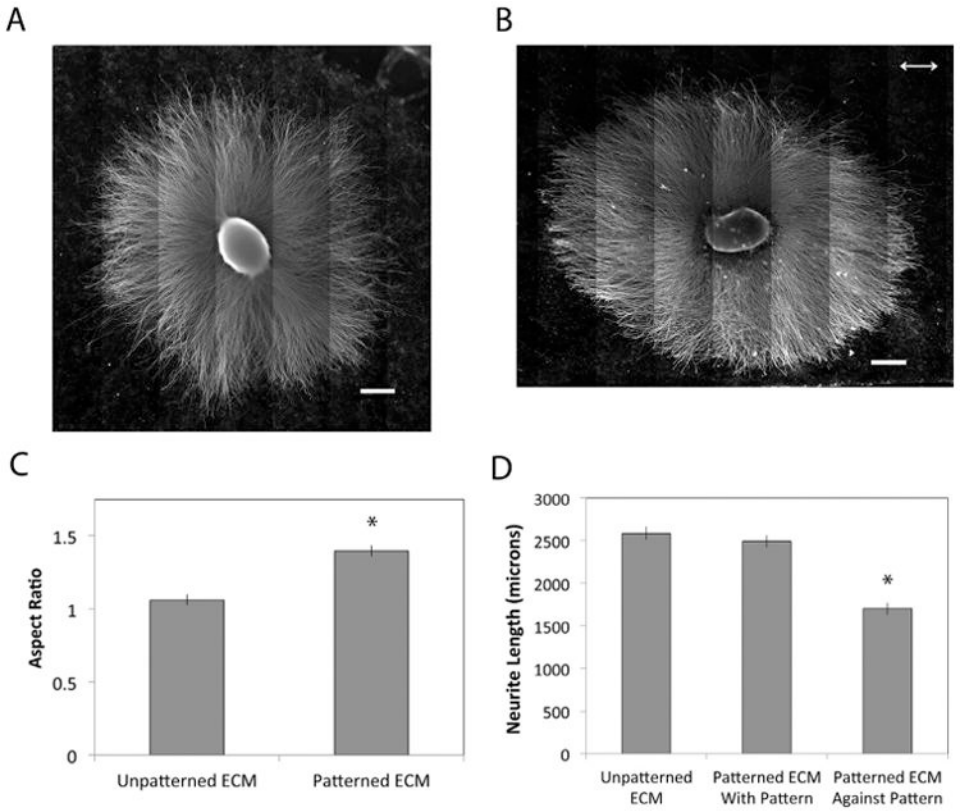

Fig. 7.

SCG explants on patterned decellularized ECM. SCG explants were placed onto (A) unpatterned and (B) patterned decellularized ECM and cultured for 3 days to allow neurite outgrowth. Double headed arrow indicates the direction of the striped pattern. Scale bars are 500 microns. (C) Neurite outgrowth was quantified by fitting outgrowth area to an ellipse and calculating the aspect ratio of the ellipse. Aspect ratios for 3 explants were averaged. (D) Average neurite lengths were determined by fitting outgrowth to an ellipse, measuring neurites in four directions, and averaging the values for neurites parallel to the pattern and for neurites perpendicular to the pattern. Average neurite lengths from 3 patterned explants were plotted against averages from unpatterned explants (calculated as described in Section 4.5). Results ± standard error is shown. * $p < 0.05$.